Optical Properties of Helical Cylindrical Molecular Aggregates: The Homogeneous Limit

Cătălin Didraga,[†] Joost A. Klugkist,[†] and Jasper Knoester*[,†,‡]

Institute for Theoretical Physics and Materials Science Centre, University of Groningen, Nijenborgh 4, 9747 AG Groningen, The Netherlands, and Department of Chemistry, Massachusetts Institute of Technology, Cambridge, Massachusetts 02139

Received: May 31, 2002; In Final Form: August 22, 2002

Using a Frenkel exciton model, we study the optical absorption spectrum and linear and circular dichroism (CD) spectra of cylindrical molecular aggregates. We demonstrate that such aggregates can always be described as a stack of molecular rings with nearest-neighbor rings rotated relative to each other by a helical angle γ. For homogeneous aggregates, the cylindrical symmetry allows for a decomposition of the Hamiltonian into a set of effective one-dimensional Hamiltonians, which are characterized by a transverse wavenumber k_2. The helical nature of the cylinder renders these Hamiltonians complex and noninversion symmetrical in general. Only the bands with $k_2 = 0$ and $k_2 = \pm 1$ are dipole-allowed and yield contributions to the various linear spectra studied. The k_2 decomposition also allows for a convenient separation of the CD into ring and helical contributions, which in turn allows us to explain the strong sensitivity of this spectrum to various system parameters, such as the molecular orientations and the ratio of cylinder length and circumference. The latter is explicitly demonstrated by numerically studying the size dependence of the spectra for chlorosomes of green bacteria. The results suggest that the strong variation of the CD as reported experimentally may result from size variations. We also present analytical results valid for long cylinders. In this case, we find three superradiant states to be responsible for the complete linear optical response: one at total wave vector $\mathbf{k} = \mathbf{0}$ and the other two (degenerate) at wave vectors determined by the circumference and the helical angle γ.

I. Introduction

Lately, an increased interest has emerged in the optical properties and exciton dynamics of molecular aggregates with a cylindrical geometry. Such aggregates exist as unique light-harvesting systems in the chlorosomes of green photosynthetic bacteria; thousands of bacteriochlorophyll (BChl) molecules form self-assembled rod-shaped supramolecular antenna systems, which are responsible for the absorption of sunlight and the transport of its energy in the form of excitons to the photosynthetic reaction centers in the base plate of the chlorosomes.[1] Many spectroscopic studies have been carried out on chlorosomes, and various models for their structure have been proposed.[2−12] On the basis of various kinds of spectroscopy and molecular modeling, a detailed model for the organization of the BChl molecules in the rods has been proposed for the chlorosomes of *Chloroflexus aurantiacus* and *Chlorobium tepidum*.[13−16] In this model, the molecules form a cylinder with a diameter of ∼5 nm (*Chlorofexus*) or ∼10 nm (*Chlorobium*) and a length that may reach several hundreds of nanometers. The proposed structure is helical and may be viewed as (interacting) strands of molecules that wind around the cylinder. In the traditional language of molecular aggregates, these systems should be referred to as J aggregates, as their absorption band is red-shifted relative to that of a single BChl molecule.

Interestingly, it has very recently been demonstrated that cylindrical J aggregates can also be prepared through a self-assembly process in a solution of cyanine dye molecules substituted with amphiphilic groups.[17,18] Cryogenic transmission electron microscopy reveals the formation of cylindrical structures with diameters in the order of 10 nm and a length that may reach micrometers. These cylinders also appear to have a helical organization, although a detailed molecular picture based on direct microscopy is not available at the moment. The linear optical properties of these aggregates are consistent with a cylindrical shape and have been used to estimate the cylinder circumference.[19,20] Pump−probe spectroscopy has been used to characterize the exciton length scale in the longitudinal direction, i.e., parallel to the cylinder axis.[20,21] In total, the excitons on these cylinders were reported to delocalize over ∼100 molecules at low temperature,[20,21] which happens to be of the same order of magnitude as the delocalization reported for the chlorosomal aggregates.[22] It should be emphasized that this number is a rough estimate, due to the uncertainty in the molecular organization within the cyanine cylinders. A more detailed characterization and better control[23] of the growth, structure, and optical dynamics of these aggregates are of great interest for the formation of artificial light-harvesting complexes. Cyanine dyes are among the molecules with the highest observed absorbance and the best aggregation properties due to their polymethine electronic structure.[24] This also underlies the success of cyanine dyes and their aggregates as photographic sensitizers.[25−27] It is conceivable that their light-harvesting properties may be made superior to the natural chlorophyll-based systems.

The aim of this paper is a theoretical study of the linear optical properties of cylindrical molecular aggregates. Our previous work of these properties,[20,28] mainly inspired by the experiments performed on the cyanine aggregates, was limited to the simplest possible model, where the organization of the molecules was taken to be nonhelical (though the dipolar orientations did add

* To whom correspondence should be addressed. Fax: 31-50-3634947. E-mail: knoester@phys.rug.nl.
[†] University of Groningen.
[‡] Massachusetts Institute of Technology.

10.1021/jp026217s CCC: $22.00
Published on Web 10/15/2002

a certain helicity to the system) and the intermolecular transfer interactions were limited to a few nearest neighbors. It is important, however, to go beyond this first step and to wonder in particular how an explicit helicity and long-range dipole−dipole interactions affect the spectra. For chlorosomes, where a detailed structural model is available,[13,14] this may be done without introducing additional free parameters. For the cyanine cylinders, one may hope that soon a better characterization of their structure, for instance using NMR, becomes available as well.

We will thus study the linear spectra for the most general cylinder structure. A second generalization over our previous work is that in addition to the linear absorption spectrum, we will also study the linear dichroism (LD) and circular dichroism (CD) spectra, which are generally very useful to extract additional information concerning the intermolecular interactions and the organization of the molecular dipole moments in molecular aggregates.[29] Actually, the CD spectrum of chlorosomes is a much debated observable, as various reports strongly differ, even qualitatively, in the measured spectra.[2,3,5−10] As a possible explanation, Somsen et al.,[30] using a spectral moment analysis for cylindrical aggregates with periodic boundary conditions, showed that the CD is very sensitive to the orientation of the molecules within the cylinder. While it is unclear whether there is sufficient freedom for the molecular orientations in the self-assembled chlorosomes with a very tight network of hydrogen bonds[13] to explain the observed variation of the CD, the result of Somsen et al. is a manifestation of a more general property, which we will demonstrate in this paper. We will show that the CD of helical cylindrical aggregates is very sensitive to the details of the band structure at the bottom of the exciton band (much more sensitive than the absorption spectrum). This structure may be modified by changing molecular orientations within the aggregate, by altering the helical angle of the structure, but also by changing the length of the cylinder. The latter seems a parameter that is easily affected by the preparation route in experimental studies and may be a more natural explanation of the observed variation.[22] As length dependence cannot be studied in a reliable way by using periodic boundary conditions, we will in the general setup of our analysis not use them. A model for the rod elements of chlorosomes that does take into account the finite rod length was also put forward by Fetisova et al.,[31] formulated in terms of Davydov components. The exciton wave functions presented by these authors, however, do not properly account for long-range interactions; moreover, the model does not include helicity of the structure.

Like most of the previous work on cylindrical aggregates, we will neglect the role of disorder. Although this is a limitation of the present work, a number of reasons justify this. First, as the cylinders have a second propagation dimension for the excitons, the localizing role of disorder is less dramatic than in the abundantly studied one-dimensional (1D) J aggregates. Second, even in the case of 1D aggregates, model studies for (almost) homogeneous systems have proven to be very useful to formulate the important concepts, like exchange narrowing,[32−34] superradiance (selection rules),[35−37] and Pauli exclusion.[38−40] These concepts have appeared to remain valid even in the presence of disorder, provided that the physical aggregate length is replaced by the exciton delocalization size.[33,41−43] We believe that similarly a proper understanding of the properties of homogeneous cylindrical aggregates should precede a detailed study of disorder (which will be the subject of a future publication). Finally, the work by Griebenow et al.[6] and recent work of Prokhorenko and Holzwarth[22] suggest that for chlorosomes of *C. aurantiacus* the main absorption line at 740 nm is mainly homogeneously broadened.

We will use the cylindrical symmetry of homogeneous cylinders to decompose the total cylinder Hamiltonian into N_2 effective 1D Hamiltonians, characterized by the transverse wavenumber k_2 (N_2 is the number of molecules that occur on a ring perpendicular to the cylinder axis). The effective Hamiltonians are generally complex and do not obey inversion symmetry. This reflects the helical nature of the systems. The decomposition is convenient from a computational point of view, as it reduces the size of the exciton Hamiltonian to be diagonalized by a factor of N_2. More importantly, certain selection and classification rules for the absorption, LD, and CD spectra are easily formulated in terms of k_2. It turns out that only two effective Hamiltonians have to be explicitly diagonalized, namely, the one with $k_2 = 0$ and the one with $k_2 = 1$. We present general expressions for the three types of spectra in terms of the solutions to these two eigenvalue problems. We use these expressions to calculate numerically the spectra for chlorosomes as a function of the cylinder length. In addition, we derive analytical expressions for the spectra in the presence of periodic boundary conditions in the longitudinal direction of the cylinder and for the situation where the effective Hamiltonians have only (complex) nearest-neighbor interactions. The analysis with periodic boundary conditions properly recovers the numerically obtained spectra for long cylinders and shows that in that limit only three superradiant exciton states determine the complete linear optical response. The structural helicity of the cylinder plays a crucial rule in two of these superadiant states.

The outline of this paper is as follows. In Section II, we first explain the general description of cylindrical aggregates in terms of a helical stack of rings. Next, we present the exciton model and the reduction to effective 1D Hamiltonians. In Section III, we give the formal expressions for the three types of spectra studied, derive the selection rules, and give the general expressions for the spectra in terms of the two 1D problems mentioned above. Section IV is dedicated to the analytical results obtained for periodic boundary conditions and effective nearest-neighbor interactions. Numerical results as a function of cylinder length are presented in Section V, together with a discussion of their implication for the interpretation of experiments on chlorosomes. We also briefly discuss the validity of the analytical results. Finally, in Section VI, we conclude.

II. Model and Reduction to Effective 1D Hamiltonians

We consider a cylindrical aggregate consisting of N molecules occupying a two-dimensional (2D) lattice that has been rolled onto a cylinder surface. We will restrict ourselves to the situation of one molecule per unit cell; the generalization is straightforward. Before turning to the Hamiltonian, we specify the geometry in more detail. Let us denote the basis vectors of the lattice by $\mathbf{a}_1$ and $\mathbf{a}_2$, as in Figure 1. Now, we form the aggregate by rolling the lattice in a certain direction given by the vector $\mathbf{C}$ and by identifying beginning and end points of $\mathbf{C}$ with each other. In analogy to the literature on carbon nanotubes, we refer to the vector $\mathbf{C}$ as the chiral vector.[44] Clearly, the various choices for $\mathbf{C}$ generate the various ways in which the cylinder can be constructed. Because for a consistent rolling, $\mathbf{C}$ should connect two lattice points, we have $\mathbf{C} = c_1\mathbf{a}_1 + c_2\mathbf{a}_2$ (c_1 and c_2 integer); the absolute value of the chiral vector equals the cylinder's circumference, $|\mathbf{C}| = 2\pi R$, with R the radius of the cylinder. Finally, $\mathbf{C}$ is perpendicular to the axis of the cylinder, which we will refer to as the z-axis.

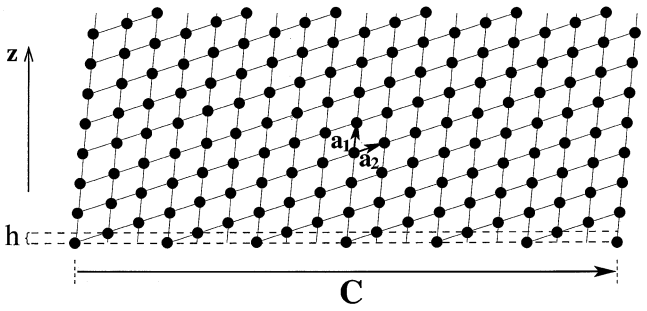

Figure 1. Construction of a cylindrical aggregate starting from a 2D lattice with primitive vectors $\mathbf{a}_1$ and $\mathbf{a}_2$. Each lattice site is occupied by a molecule. The lattice is rolled onto a cylinder in the direction indicated by the chiral vector **C** and with circumference given by $|\mathbf{C}|$. Beginning and end points of the chiral vector are identified with each other. The axis of the cylinder is referred to as the *z*-axis. After the rolling process, the aggregate may be viewed as a stack of rings, separated from each other by a distance h and occupied by a number N_2 of molecules at regular distances. Neighboring rings are rotated around the *z*-axis by a helical angle $\gamma = 2\pi \max(|\mathbf{C}\cdot\mathbf{a}_1|; |\mathbf{C}\cdot\mathbf{a}_2|)/\mathbf{C}^2$ (see Figure 2).

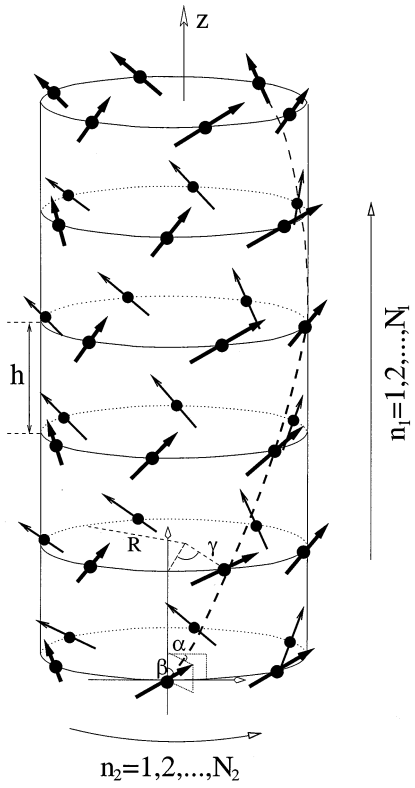

Figure 2. Cylindrical aggregate obtained from rolling a 2D lattice, as in Figure 1. The aggregate consists of a stack of N_1 rings, labeled $n_1 = 1, 2, ..., N_1$, that each contain N_2 molecules, labeled $n_2 = 1, 2, ..., N_2$. The arrows indicate the transition dipoles, which are equal in magnitude (μ) and make an angle β with the cylinder axis. The projection of each dipole on the plane of the rings makes an angle α with the local tangent to the ring. Each ring is rotated with respect to the previous one over an angle γ, so that we may view the aggregate as a collection of N_2 parallel helices on the cylinder's surface. One such helix is indicated by the dashed curve. The label n_2 in fact labels the helices.

Having constructed the cylinder, we can look at it in a slightly different way, which turns out to be more useful when diagonalizing the Hamiltonian. Let us denote by N_2 the number of lattice sites (i.e., molecules) crossed by the chiral vector (not double-counting beginning and end points, i.e, $N_2 = 6$ for the example of Figure 1). As a result of the periodicity of the 2D lattice, these N_2 sites will be placed equidistantly on a ring of radius R. The same holds for all sets of sites that have a certain given distance to the chiral vector. We will denote the distance between two such neighboring sets by h (see Figure 1). We conclude that we may also view a general cylindrical aggregate as a stack of rings, each with radius R and occupied by N_2 molecules, and with a separation between nearest rings given by h. The total number of rings stacked in this way will be denoted N_1 (which equals 24 for the example of Figure 1). It is important to note that the relative positions of the N_2 molecules on two neighboring rings are shifted along the ring with the "helicity" angle $\gamma = 2\pi \max(|\mathbf{C}\cdot\mathbf{a}_1|; |\mathbf{C}\cdot\mathbf{a}_2|)/\mathbf{C}^2$ (Figure 2). The angle γ can take values between 0 and $2\pi/N_2$; larger or negative values can always be mapped into this interval. Having identified the cylinder with a helical stack of rings, we will from now on label the molecules with the coordinates $\mathbf{n} = (n_1, n_2)$, where $n_1 = 1, 2, ..., N_1$ labels the ring and $n_2 = 1, 2, ..., N_2$ labels the helix on which the molecule lies. One of these helices has been indicated by the dashed curve in Figure 2. The total number of molecules is now given by $N = N_1N_2$. We stress that (in general) $\mathbf{n} = (n_1, n_2)$ does not coincide with the vector that specifies the position of the molecule on the underlying 2D lattice in terms of lattice vectors $\mathbf{a}_1$ and $\mathbf{a}_2$.

We now turn to the description of the molecules and the electronic Hamiltonian. All molecules are modeled as identical two-level systems, which are nonpolar and have transition dipoles $\boldsymbol{\mu}_\mathbf{n}$ that are equal in magnitude (μ) and have equal orientations relative to the frame of the cylinder at the position of the molecule. In particular, all molecular dipoles make an angle β with the cylinder axis, while the projection of each dipole on the *xy* plane (perpendicular to this axis) makes an angle α with the local tangent to the rings that build up the cylinder. Explicitly, the *x*, *y*, and *z* components of the molecular position vectors and dipole moments are given by the three-dimensional vectors:

$$\mathbf{r}_\mathbf{n} = (R\cos(n_2\phi_2 + n_1\gamma), R\sin(n_2\phi_2 + n_1\gamma), n_1h) \quad (1)$$

$$\boldsymbol{\mu}_\mathbf{n} = (-\mu\sin\beta\,\sin(n_2\phi_2 + n_1\gamma - \alpha), \mu\sin\beta\,\cos(n_2\phi_2 + n_1\gamma - \alpha), \mu\cos\beta) \quad (2)$$

with $\phi_2 = 2\pi/N_2$.

The electronically excited states of the system are described by the Frenkel exciton Hamiltonian. Setting $\hbar = 1$, we have

$$H = \omega_0 \sum_\mathbf{n} b_\mathbf{n}^\dagger b_\mathbf{n} + \sum_{\mathbf{n},\mathbf{m}}{}' J(\mathbf{n} - \mathbf{m}) b_\mathbf{n}^\dagger b_\mathbf{m} \quad (3)$$

where $b_\mathbf{n}^\dagger$ and $b_\mathbf{n}$ denote the Pauli operators for creation and annihilation of an excitation on molecule **n**, respectively.[45,46] Furthermore, ω_0 is the molecular transition frequency and $J(\mathbf{n} - \mathbf{m})$ is the excitation transfer interaction between molecules **n** and **m**. Because of the symmetry of the system, the interaction only depends on the relative positions of the two molecules. The prime on the summation indicates that the term with $\mathbf{n} = \mathbf{m}$ is excluded from the summation. We assume that $J(\mathbf{n} - \mathbf{m})$ results from dipole−dipole interactions, giving it the explicit form

$$J(\mathbf{n} - \mathbf{m}) = \frac{\boldsymbol{\mu}_\mathbf{n}\cdot\boldsymbol{\mu}_\mathbf{m}}{|\mathbf{r}_\mathbf{nm}|^3} - 3\frac{(\boldsymbol{\mu}_\mathbf{n}\cdot\mathbf{r}_\mathbf{nm})(\boldsymbol{\mu}_\mathbf{m}\cdot\mathbf{r}_\mathbf{nm})}{|\mathbf{r}_\mathbf{nm}|^5} \quad (4)$$

with $\mathbf{r}_\mathbf{nm} = \mathbf{r}_\mathbf{n} - \mathbf{r}_\mathbf{m}$.

To diagonalize the Hamiltonian, it is convenient to first realize that the cylindrical symmetry dictates a Bloch form for the wave functions along the ring (n_2) directions. We thus make the transformation

$$c^{\dagger}_{n_1,k_2} = \frac{1}{\sqrt{N_2}} \sum_{n_2} e^{ik_2\phi_2 n_2} b^{\dagger}_{\mathbf{n}} \tag{5}$$

with k_2 the wavenumber of the Bloch state in the ring (transverse wavenumber), which takes the values $k_2 = 0, \pm 1, \pm 2, ..., \pm(N_2/2 - 1), N_2/2$ for N_2 even ($k_2 = 0, \pm 1, \pm 2, ..., \pm(N_2 - 1)/2$ for N_2 odd). After this transformation, the Hamiltonian decouples into N_2 effective 1D problems:

$$H = \sum_{k_2} H(k_2) \tag{6}$$

with

$$H(k_2) = \omega_0 \sum_{n_1} c^{\dagger}_{n_1,k_2} c_{n_1,k_2} + \sum_{n_1,m_1} J(n_1 - m_1; k_2) c^{\dagger}_{n_1,k_2} c_{m_1,k_2} \tag{7}$$

Here

$$J(n_1; k_2) = \sum_{n_2}{}' J(n_1, n_2) e^{-ik_2\phi_2 n_2} \tag{8}$$

whose physical meaning is the total transfer interaction between all molecules of two rings that are separated by $n_1 h$ and that both reside in their Bloch state with momentum k_2.

$H(k_2)$ is the effective Hamiltonian coupling N_1 rings, each in its k_2 Bloch state. Of course, $H(k_2)$ is hermitian for all k_2. Furthermore, $J(n_1; k_2)$ has the property:

$$J(n_1; k_2) = J(-n_1; -k_2) = J^*(n_1; -k_2) \tag{9}$$

where we have used eq 8 and the inversion symmetry $J(\mathbf{n}) = J(-\mathbf{n})$. Because in general $J(n_1, n_2) \neq J(n_1, -n_2)$ (helicity), we also have $J(-n_1; k_2) \neq J(n_1; k_2)$, which means that the $H(k_2)$ is generally not inversion symmetric. Inversion symmetry only holds for $k_2 = 0$; all other $H(k_2)$ values are complex with their matrix elements obeying

$$H_{n_1,m_1}(k_2) = H^*_{n_1,m_1}(-k_2) \tag{10}$$

This implies that $H(k_2)$ and $H(-k_2)$ have the same set of eigenvalues, while their corresponding eigenvectors are each other's complex conjugate. More explicitly, let us assume that $\varphi_{k_1}(n_1; k_2)$ is the n_1th component of the k_1th eigenvector of $H(k_2)$, with eigenvalue E_{k_1,k_2}. Then, $\varphi^*_{k_1}(n_1; k_2)$ is an eigenvector of $H(-k_2)$ with the same eigenvalue E_{k_1,k_2}. This allows us to focus on $H(k_2)$ with $k_2 \geq 0$, as all other eigenvectors and eigenvalues follow from those. The above also means that all eigenvalues are at least 2-fold degenerate.

Using the label $\mathbf{k} = (k_1, k_2)$ for the total exciton eigenstate, we can write

$$|\mathbf{k}\rangle = \sum_{\mathbf{n}} \varphi_{\mathbf{k}}(\mathbf{n}) b^{\dagger}_{\mathbf{n}} |g\rangle \tag{11}$$

with $|g\rangle$ the overall ground state (with all molecules in their ground state) and

$$\varphi_{\mathbf{k}}(\mathbf{n}) = \frac{1}{\sqrt{N_2}} e^{ik_2\phi_2 n_2} \varphi_{k_1}(n_1; k_2) \qquad (k_2 > 0) \tag{12}$$

For $k_2 < 0$, we will define

$$\varphi_{\mathbf{k}}(\mathbf{n}) \equiv \frac{1}{\sqrt{N_2}} e^{ik_2\phi_2 n_2} \varphi^*_{k_1}(n_1; -k_2) \qquad (k_2 < 0) \tag{13}$$

We will assume that the wave functions $\varphi_{k_1}(n_1; k_2)$ are normalized according to $\sum_{n_1} |\varphi_{k_1}(n_1; k_2)|^2 = 1$, which guarantees the normalization of the exciton states eqs 12 and 13.

As we will show in the following section, the only excitons with linear optical activity (whether absorption, LD, or CD) are those in the bands with $k_2 = 0$ and $k_2 = \pm 1$ (degenerate). Hence, calculating these linear optical spectra involves the diagonalization of the two effective 1D ($N_1 \times N_1$) problems, instead of one big $N \times N$ diagonalization. This considerably simplifies the numerical effort of the problem. Moreover, the separation into k_2 bands adds important general insight into the nature of the eigenstates.

III. Absorption, LD, and CD Spectra: General Aspects

The standard derivation of the three linear optical spectra of our interest makes use of the Fermi golden rule, i.e., first-order perturbation theory in the interaction between light and matter

$$V = -\sum_{\mathbf{n}} \boldsymbol{\mu}_{\mathbf{n}} \cdot \mathbf{E}(\mathbf{r}_{\mathbf{n}}) (b_{\mathbf{n}} + b^{\dagger}_{\mathbf{n}}) \tag{14}$$

with $\mathbf{E}(\mathbf{r_n})$ the electric field vector at position $\mathbf{r_n}$ of molecule $\mathbf{n}$. We will not repeat this derivation here but give the well-known general results in terms of the exciton eigenstates and reduce the resulting expressions further using the cylinder geometry and the k_2 decomposition introduced in Section II.

A. Linear Absorption. In the case of linear absorption, we consider a linearly polarized electromagnetic field with electric polarization direction $\mathbf{e}$ and frequency $\omega = 2\pi c/\lambda$ (c is the velocity of light, and λ is the wavelength of the field). We will assume that the spectrum is taken in an isotropic solution; that is, the measured spectrum contains an isotropic average over all possible orientations of $\mathbf{e}$ relative to the x, y, z frame of the cylinder. The spectrum is then given by

$$A(\omega) = \sum_{\mathbf{k}} O_{\mathbf{k}} \delta(\omega - E_{\mathbf{k}}) \tag{15}$$

with, to lowest order in L/λ (L is the linear dimensions of the cylinder)

$$O_{\mathbf{k}} = \langle |\sum_{\mathbf{n}} \varphi_{\mathbf{k}}(\mathbf{n}) \boldsymbol{\mu}_{\mathbf{n}} \cdot \mathbf{e}|^2 \rangle = \sum_{\mathbf{n},\mathbf{m}} \varphi_{\mathbf{k}}(\mathbf{n}) \varphi^*_{\mathbf{k}}(\mathbf{m}) \langle (\boldsymbol{\mu}_{\mathbf{n}} \cdot \mathbf{e})(\boldsymbol{\mu}_{\mathbf{m}} \cdot \mathbf{e}) \rangle \tag{16}$$

with $\langle ... \rangle$ representing orientational average. The spectrum is a series of peaks at exciton eigenfrequencies, with weights given by the oscillator strengths. From eq 16 and the completeness of the set of exciton states (closure), it follows immediately that the oscillator strengths obey the sum rule $\sum_{\mathbf{k}} O_{\mathbf{k}} = N\mu^2/3$, irrespective of the geometry of the system and the intermolecular interactions.

For our cylinders, we have

$$\langle (\mathbf{e} \cdot \boldsymbol{\mu}_{\mathbf{n}})(\mathbf{e} \cdot \boldsymbol{\mu}_{\mathbf{m}}) \rangle = (1/3)\mu^2 \cos^2\beta + (1/3)\mu^2 \sin^2\beta \cos[(n_2 - m_2)\phi_2 + (n_1 - m_1)\gamma] \tag{17}$$

Substituting this into eq 16 and performing the summation over n_2 and m_2 (using eqs 12 and 13), one finds that only the exciton bands with $k_2 = 0$ and $k_2 = \pm 1$ contain states with oscillator strength:

$$O_{\mathbf{k}} = \frac{N_2\mu^2\cos^2\beta}{3}\delta_{k_2,0}\left|\sum_{n_1}\varphi_{k_1}(n_1;0)\right|^2 + \frac{N_2\mu^2\sin^2\beta}{6}\times \left(\delta_{k_2,1}\left|\sum_{n_1}\varphi_{k_1}(n_1;1)e^{-in_1\gamma}\right|^2 + \delta_{k_2,-1}\left|\sum_{n_1}\varphi^*_{k_1}(n_1;1)e^{in_1\gamma}\right|^2\right) \quad (18)$$

Substituting this result into eq 15 and using $E_{k_1,-k_2} = E_{k_1,k_2}$, we arrive at

$$A(\omega) = \frac{\cos^2\beta}{3}\sum_{k_1} M(k_1,0)\delta(\omega - E_{k_1,0}) + \frac{\sin^2\beta}{3}\sum_{k_1} M(k_1,1)\delta(\omega - E_{k_1,1}) \quad (19)$$

with

$$M(k_1,k_2) = N_2\mu^2\left|\sum_{n_1}\varphi_{k_1}(n_1;k_2)e^{-in_1k_2\gamma}\right|^2 \quad (20)$$

We thus find that the linear absorption spectrum shows two sets of peaks. One set results from states in the $k_2 = 0$ band and is polarized parallel to the axis of the cylinder ($\cos^2\beta$); the other results from the $k_2 = \pm 1$ bands and are polarized perpendicular to the cylinder axis ($\sin^2\beta$). The $k_2 = \pm 1$ bands give equal contributions due to their degeneracy. The weight $M(k_1, k_2)$ can be interpreted as the oscillator strength of the exciton $\mathbf{k}$ for light polarized in the direction of the exciton's transition dipole.

B. LD. Linear dichroism is the difference in absorption spectrum for two beams of linearly polarized light of which the polarization vectors are mutually perpendicular. The spectrum vanishes in an isotropic solution and is therefore taken in an oriented sample. We will consider a sample in which the cylinders have been oriented with their axes parallel to each other. The LD is then given by

$$LD(\omega) = A_{\parallel}(\omega) - A_{\perp}(\omega) \quad (21)$$

where $A_{\parallel}(\omega)$ and $A_{\perp}(\omega)$ are the absorption spectra for light polarized, respectively, along and perpendicular to the cylinder axes. In direct analogy to the absorption spectrum, the LD spectrum reads

$$LD(\omega) = \sum_{\mathbf{k}} L_{\mathbf{k}}\delta(\omega - E_{\mathbf{k}}) \quad (22)$$

with

$$L_{\mathbf{k}} = \sum_{\mathbf{n},\mathbf{m}}\varphi_{\mathbf{k}}(\mathbf{n})\varphi^*_{\mathbf{k}}(\mathbf{m})\left[(\boldsymbol{\mu}_{\mathbf{n}}\cdot\mathbf{z})(\boldsymbol{\mu}_{\mathbf{m}}\cdot\mathbf{z}) - \langle(\boldsymbol{\mu}_{\mathbf{n}}\cdot\mathbf{e}_{\perp})(\boldsymbol{\mu}_{\mathbf{m}}\cdot\mathbf{e}_{\perp})\rangle\right] \quad (23)$$

where in the last term $\langle\ldots\rangle$ denotes the average of the polarization vector $\mathbf{e}_{\perp}$ over all orientations within the xy plane of the cylinders. Using steps similar to the ones performed for the absorption spectrum, one finds again that only the exciton bands with $k_2 = 0$ and $k_2 = \pm 1$ contribute to the LD spectrum. One thus eventually arrives at

$$LD(\omega) = \cos^2\beta\sum_{k_1} M(k_1,0)\delta(\omega - E_{k_1,0}) - \frac{\sin^2\beta}{2}\sum_{k_1} M(k_1,1)\delta(\omega - E_{k_1,1}) \quad (24)$$

The LD spectrum obeys the sum rule $\int d\omega LD(\omega) = \sum_{\mathbf{k}} L_{\mathbf{k}} = N\mu^2(3\cos^2\beta - 1)/2$. Combining this with the integral of the absorption spectrum in an isotropic medium ($N\mu^2/3$) allows one in principle to measure the angle β. This technique relies strongly on a good alignment of the cylinders; for misalignment, it overestimates β.[4]

C. CD. The CD spectrum is the difference in absorption spectrum for left (L) and right (R) circularly polarized light:

$$CD(\omega) = A_{\mathrm{L}}(\omega) - A_{\mathrm{R}}(\omega) \quad (25)$$

The CD spectrum is usually taken in an isotropic sample. It may be calculated using the Fermi golden rule with the interaction eq 14, where the electric field is taken either left polarized or right polarized (see refs 47 and 48 for definitions). This yields

$$CD(\omega) = \sum_{\mathbf{k}} R_{\mathbf{k}}\delta(\omega - E_{\mathbf{k}}) \quad (26)$$

with $R_{\mathbf{k}}$ the rotational strength, which in an isotropic sample vanishes to zeroth order in L/λ. The first-order contribution reads

$$R_{\mathbf{k}} = \frac{1}{3}\frac{\pi}{2\lambda}\sum_{\mathbf{nm}}\varphi_{\mathbf{k}}(\mathbf{n})\varphi^*_{\mathbf{k}}(\mathbf{m})\mathbf{r}_{\mathbf{nm}}\cdot(\boldsymbol{\mu}_{\mathbf{n}}\times\boldsymbol{\mu}_{\mathbf{m}}) \quad (27)$$

Here, $\mathbf{r}_{\mathbf{nm}}$ is as defined below eq 4. The derivation can be found in ref 30, which we slightly generalized by allowing for complex wave functions. Using the closure relation for the exciton wave functions, one easily shows that $\sum_{\mathbf{k}} R_{\mathbf{k}} = 0$, which means that the integral of the CD over all frequencies vanishes. This property is referred to as the CD being conservative.

Using $\mathbf{r}_{\mathbf{nm}}$ and $\boldsymbol{\mu}_{\mathbf{n}}$ as defined in Section II, we arrive at

$$\mathbf{r}_{\mathbf{nm}}\cdot(\boldsymbol{\mu}_{\mathbf{n}}\times\boldsymbol{\mu}_{\mathbf{m}}) = R\mu^2\sin 2\beta\cos\alpha\{1 - \cos[(n_2 - m_2)\phi_2 + (n_1 - m_1)\gamma]\} - h(n_1 - m_1)\mu^2\sin^2\beta\sin[(n_2 - m_2)\phi_2 + (n_1 - m_1)\gamma] \quad (28)$$

Substituting this into eq 27, using eqs 12 and 13, and performing the summation over n_2 and m_2, we again find that only the bands with $k_2 = 0, \pm 1$ contribute to the CD. Explicitly, we have

$$R_{\mathbf{k}} = \frac{\sin 2\beta\cos\alpha}{3}\frac{\pi R}{2\lambda}\left[\delta_{k_2,0}M(k_1,0) - \frac{1}{2}(\delta_{k_2,1} + \delta_{k_2,-1})M(k_1,1)\right] + \frac{\sin^2\beta}{6}\frac{\pi h}{2\lambda}(\delta_{k_2,1} + \delta_{k_2,-1})W(k_1,1) \quad (29)$$

with

$$W(k_1,1) = \frac{N_2\mu^2}{\mathrm{i}}\sum_{n_1,m_1}[(n_1 - m_1)e^{-\mathrm{i}(n_1-m_1)\gamma}\varphi_{k_1}(n_1;1)\times \varphi^*_{k_1}(m_1;1)] \quad (30)$$

One easily shows that $W(k_1, 1)$ is real. Substituting eq 29 into eq 26 and using $E_{k_1,1} = E_{k_1,-1}$, one arrives at

$$CD(\omega) = \frac{\sin 2\beta\cos\alpha}{3}\frac{\pi R}{2\lambda}\left[\sum_{k_1} M(k_1,0)\delta(\omega - E_{k_1,0}) - \sum_{k_1} M(k_1,1)\delta(\omega - E_{k_1,1})\right] + \frac{\sin^2\beta}{3}\frac{\pi h}{2\lambda}\sum_{k_1} W(k_1,1)\delta(\omega - E_{k_1,1}) \quad (31)$$

The first two terms in eq 31 have opposite signs and equal weights because $\sum_{k_1} M(k_1, 0) = \sum_{k_1} M(k_1, 1) = N\mu^2$. These two terms together closely resemble the S-shaped CD spectrum of a single ring aggregate[29] and will therefore be referred to as the "ring" contribution. The third term closely resembles the CD spectrum of a single stack (straight line) of molecules with their dipoles winding around the line in a helical way and will therefore be referred to as the "helical" contribution. The distinction between these type of contributions was also made in ref 30 for the special case where periodic boundary conditions are applied in the n_1 direction (Section IV, A). The integral of the helical contribution over all frequencies vanishes, as immediately follows from the conservative nature of the total CD and the fact that the ring contributions have zero net weight. Alternatively, the conservative nature of the helical contribution is easily shown explicitly by performing $\sum_{k_1} W(k_1, 1)$, using the closure relation of the $\varphi_{k_1}(n_1; 1)$.

We finally note that the ratio of the ring and helical terms in the total CD spectrum is proportional to $(2R/h)\cot\beta\cos\alpha$ and thus strongly depends on the geometrical parameters. Moreover, this ratio depends on N_1, N_2, and γ through the moments $M(k_1, 0)$, $M(k_1, 1)$, and $W(k_1, 1)$.

IV. Analytical Results

In this section, we give analytical expressions for the three types of spectra. We first derive such expressions by imposing periodic boundary conditions in the n_1 direction, an approach that should hold for long cylinders (N_1 large). A second set of analytical spectra is obtained by restricting the interring interactions to nearest-neighbor ones.

A. Periodic Boundary Conditions. If we impose periodic boundary conditions in the n_1 direction, the eigenfunctions of the effective 1D Hamiltonians $H(k_2)$ should assume a Bloch form, independent of k_2. Introducing $\phi_1 = 2\pi/N_1$, we thus have

$$\varphi_{k_1}(n_1; k_2) = \frac{1}{\sqrt{N_1}} e^{ik_1\phi_1 n_1} \tag{32}$$

for $k_2 > 0$, while for $k_2 < 0$ we define $\varphi_{k_1}(n_1; k_2) = \varphi^*_{k_1}(n_1; -k_2)$, in accordance with the convention introduced in Section II. Here, $k_1 = 0, \pm1, \pm2, ..., \pm(N_1/2 - 1), N_1/2$ for N_1 even ($k_1 = 0, \pm1, \pm2, ..., \pm(N_1 - 1)/2$ for N_1 odd). Combining $\varphi_{k_1}(n_1; k_2)$ with eq 12, we know the total exciton wave function. The corresponding energy is given by

$$E_{\mathbf{k}} = \omega_0 + \sum_{\mathbf{n}}{}' J(\mathbf{n}) \cos[k_1\phi_1 n_1 + k_2\phi_2 n_2], \text{ for } k_2 > 0 \tag{33}$$

Here, the prime excludes the term with $\mathbf{n} = 0$. For $k_2 < 0$, $E_{k_1,k_2} = E_{k_1,-k_2}$.

Substituting eq 32 into eq 19, we obtain

$$A(\omega) = \cos^2\beta \frac{N\mu^2}{3} \delta(\omega - E_{0,0}) + \sin^2\beta \frac{N\mu^2}{3} \sum_{k_1} f(k_1)\delta(\omega - E_{k_1,1}) \tag{34}$$

with

$$f(k_1) = \frac{1}{N_1^2} \frac{\sin^2[N_1(k_1\phi_1 - \gamma)/2]}{\sin^2[(k_1\phi_1 - \gamma)/2]} \tag{35}$$

We see that the linear absorption spectrum consists of one peak polarized parallel to the z-axis and many peaks, each weighted by $f(k_1)$, polarized perpendicular to the z-axis.

As periodic boundary conditions in the n_1 direction are only justified for long cylinders, we will concentrate on the large N_1 limit. In this limit, $\sum_{k_1}$ in eq 34 may be replaced by $(N_1)/(2\pi)\int_{-\pi}^{+\pi} dq$ with $q = k_1\phi_1$. We now use

$$\lim_{\epsilon\to 0} \frac{\epsilon}{\pi} \frac{\sin^2(x/\epsilon)}{\sin^2 x} = \delta(x) \text{ for } x \in \left(-\frac{\pi}{2}, \frac{\pi}{2}\right) \tag{36}$$

to find that only the contribution with $q = k_1\phi_1 = \gamma$ survives in the limit of large N_1. The total absorption spectrum then reduces to

$$A(\omega) = \frac{N\mu^2}{3} [\cos^2\beta\, \delta(\omega - E_0) + \sin^2\beta\, \delta(\omega - E_h)] \tag{37}$$

with

$$E_0 \equiv E_{0,0} = \omega_0 + \sum_{\mathbf{n}}{}' J(\mathbf{n}) \tag{38}$$

$$E_h \equiv E_{\gamma/\phi_1,1} = \omega_0 + \sum_{\mathbf{n}}{}' J(\mathbf{n}) \cos(\gamma n_1 + \phi_2 n_2) \tag{39}$$

The summations over $\mathbf{n}$ in the latter two equations must be consistent with the periodic boundary conditions, which means that they run over $n_i = 0, \pm1, \pm2, ..., \pm(N_i/2 - 1), N_i/2$ if N_i is even (for N_i odd, the last two terms are replaced by $\pm(N_i - 1)/2$).

Thus, for long cylinders, the absorption spectrum contains two peaks. The one at energy E_0 is polarized parallel to the z-axis; it is a zero-momentum state and has amplitudes that are equal to $1/\sqrt{N}$ for all molecules on the cylinder. This immediately explains the polarization of this peak, as the components of the molecular dipoles perpendicular to the z-axis, which sinusoidally vary around the cylinder, destructively interfere in this state. The peak at E_h is polarized perpendicular to the z-axis and results from two degenerate exciton transitions, which have opposite signs of k_2. The wave functions of these excitons behave like $(1/\sqrt{N})e^{\pm i(\gamma m_1 + \phi_2 m_2)}$, which we refer to as the helical exciton states, because the helical angle plays an important role in them. This name explains the subscript "h" in E_h. For this state, the components of the dipoles parallel to the z-axis destructively interfere, while the ones perpendicular to the z-axis add constructively: their variation with position is exactly balanced by the variation of the wave function. The zero momentum exciton state and the two helical ones are the superradiant states in the $N_1 \to \infty$ limit; all others become dark.

In practice, the δ peaks in the spectrum eq 37 are homogeneously and inhomogeneously broadened. In this paper, we simply incorporate such broadening effects by convoluting the above spectrum with a line shape function $F(\omega)$, which is assumed to have a simple single-peak structure, for instance a Gaussian. This yields

$$A(\omega) = \frac{N\mu^2}{3} [\cos^2\beta\, F(\omega - E_0) + \sin^2\beta\, F(\omega - E_h)] \tag{40}$$

Following steps similar to the above, one derives the LD and CD spectra for periodic boundary conditions for N_1 large. For the LD spectrum, we find

$$LD(\omega) = N\mu^2\left[\cos^2\beta\, \delta(\omega - E_0) - \frac{1}{2}\sin^2\beta\, \delta(\omega - E_h)\right] \tag{41}$$

and its straightforward modification if we include the line shape function $F(\omega)$. The spectrum exhibits a positive peak associated with the zero-momentum exciton, polarized along the cylinder axis, and a negative peak due to the two helical excitons, polarized perpendicular to the axis.

For the CD spectrum, the final result for periodic boundary conditions reads

$$CD(\omega) = \frac{N\mu^2}{3}\frac{\pi R}{2\lambda}\sin 2\beta \cos\alpha\,[\delta(\omega - E_0) - \delta(\omega - E_h)] - \frac{N\mu^2}{3}\frac{\pi h}{2\lambda}\,v_h(\gamma)\sin^2\beta\,\delta'(\omega - E_h) \quad (42)$$

with

$$v_h = \left[\frac{\mathrm{d}}{\mathrm{d}(k_1\phi_1)}E_{k_1,1}\right]_{k_1=\gamma/\phi_1} = -\sum_{\mathbf{n}} n_1 J(\mathbf{n})\sin(\gamma n_1 + \phi_2 n_2) \quad (43)$$

The quantity v_h equals the group velocity of the helical excitons in the direction along the helices, while $\delta'(\omega - E_h)$ denotes the derivative of the Dirac δ distribution at the energy of the helical exciton. This derivative can be viewed as the combination of a negative and a positive Dirac δ distribution placed infinitesimally close together, in such a way that the product of their separation and their height is constant. The result expressed by eq 42 is equivalent to the spectral moments derived in ref 30.

The first two terms in eq 42 derive from the two M terms in eq 31 in a way completely analogous to the linear absorption spectrum eq 37, while the third contribution results from the $W(k_1, 1)$ term in eq 31. The derivative comes in by realizing that

$$W(k_1, 1) = \frac{N_2\,\mu^2}{N_1\mathrm{i}}\sum_{n_1,m_1}(n_1 - m_1)e^{\mathrm{i}(k_1\phi_1-\gamma)(n_1-m_1)} = -\frac{N_2}{N_1}\mu^2\frac{\mathrm{d}}{\mathrm{d}(k_1\phi_1)}\left|\sum_{n_1}e^{\mathrm{i}(k_1\phi_1-\gamma)n_1}\right|^2 \quad (44)$$

Treating the n_1 summation in the last expression in the same way as we did for the absorption spectrum, we obtain for N_1 large the $k_1\phi_1$ derivative of the $\delta(k_1\phi_1 - \gamma)$ function in the integration over $q = k_1\phi_1$. Using partial integration, this derivative may be shifted to the energy δ function occurring in the expression for the total spectrum (cf. eq 26). Finally, replacing $\partial/\partial(k_1\phi_1)$ by $\partial/\partial\omega$ introduces the group velocity as an extra prefactor.

If we now convolute all transitions with the line shape function $F(\omega)$, we have

$$CD(\omega) = \frac{N\mu^2}{3}\frac{\pi R}{2\lambda}\sin 2\beta \cos\alpha\,[F(\omega - E_0) - F(\omega - E_h)] - \frac{N\mu^2}{3}\frac{\pi h}{2\lambda}v_h\sin^2\beta\,\frac{\mathrm{d}F(\omega - E_h)}{\mathrm{d}\omega} \quad (45)$$

We thus see that like the absorption spectrum, the ring part of the CD (the first two terms in eq 45) has two peaks, occurring at E_0 and E_h but now these peaks have opposite sign and equal weight. Which one is positive depends on the angles α and β. The helical contribution (the last term in eq 45) is centered at E_h and has (for a single-peaked $F(\omega)$) an S shape with total weight zero. Whether the positive contribution of the helical part is on the high- or low-energy side of E_h depends on the sign of v_h. The separation between the positive and the negative peaks in the helical contribution is dictated completely by the width of $F(\omega)$. On the other hand, in the ring contribution, the separation between the positive and the negative peaks is determined by the bigger one of the width of $F(\omega)$ and the energy separation $|E_h - E_0|$.

To conclude this section, we mention that one can show that the number of net peaks in the CD spectrum eq 45 is at most three if we use a Gaussian for $F(\omega)$, independent of its width. Only two peaks can be seen in certain special cases, for instance for $\alpha = \pi/2$, $\beta = \pi/2$, or $\gamma = 0$, or other cases depending on the magnitudes of v_h, the width of $F(\omega)$, and $E_h - E_0$. The CD spectrum vanishes completely if all of the transition dipole moments are parallel, i.e., if $\beta = 0$. At the end of Section V, we will discuss the convergence of the absorption, LD, and CD spectra to the large-N_1 spectra obtained above.

B. Effective Nearest-Neighbor Interactions. In this section, we do not impose periodic boundary conditions, but instead, we will assume that the effective interactions $J(n_1; k_2)$ defined in eq 8 are short-ranged, allowing us to discard them beyond the first neighboring ring. We thus have

$$J(n_1; k_2) = J(0; k_2)\delta_{n_1,0} + J(1; k_2)\delta_{n_1,1} + J^*(1, k_2)\delta_{n_1,-1} \quad (46)$$

The resulting Hamiltonian eq 7 represents a 1D system with nearest-neighbor interactions, without inversion symmetry (unless $k_2 = 0$). The analytical diagonalization of this problem for open boundary conditions in the n_1 direction gives

$$\varphi_{k_1}(n_1; k_2) = \sqrt{\frac{2}{N_1 + 1}}\exp(\mathrm{i}n_1\theta_{k_2})\sin\left(\frac{\pi k_1 n_1}{N_1 + 1}\right) \quad (47)$$

with $k_1 = 1, 2, ..., N_1$. The solution eq 47 differs from the well-known inversion−symmetric case through the phase factor $\exp(\mathrm{i}n_1\theta_{k_2})$, where θ_{k_2} is defined through $J(1; k_2) = s|J(1; k_2)|\exp(\mathrm{i}\theta_{k_2})$, with s the sign of $\mathrm{Re}J(1, k_2)$. Thus, $-\pi/2 < \theta_{k_2} \leq \pi/2$. We note that $\theta_{-k_2} = -\theta_{k_2}$, so that the above wave functions automatically obey the relation between the $\pm k_2$ states imposed in Section II. The energy of the total exciton state $|k_1, k_2\rangle$ (eq 12) is now given by

$$E_{k_1,k_2} = \omega_0 + J(0;k_2) + 2s|J(1; k_2)|\cos\left(\frac{\pi k_1}{N_1 + 1}\right) \quad (48)$$

Using the above expression for the $\varphi_{k_1}(n_1; k_2)$, one derives through straightforward algebra that

$$M(k_1, 0) = \frac{N_2\,\mu^2}{N_1 + 1}[1 - (-1)^{k_1}]\cot^2(\phi_1'/2) \quad (49)$$

$$M(k_1, 1) = \frac{N_2\mu^2}{2(N_1 + 1)}\left[\frac{\sin[N_1(\phi_1' + \gamma - \theta_1)/2]}{\sin[(\phi_1' + \gamma - \theta_1)/2]} - (-1)^{k_1}\frac{\sin[N_1(\phi_1' - \gamma + \theta_1)/2]}{\sin[(\phi_1' - \gamma + \theta_1)/2]}\right]^2 \quad (50)$$

$$W(k_1, 1) = \frac{\partial M(k_1, 1)}{\partial\gamma} \quad (51)$$

Here, we defined $\phi_1' = \pi k_1/(N_1 + 1)$. Equations 49−51 together with eqs 19, 24, and 31 yield the expressions for the stick spectra, which again may be convoluted with the line shape $F(\omega)$ to account for broadening of each of the exciton transitions.

Clearly, the resulting spectra are more complicated than in the case of periodic boundary conditions. The open boundary

conditions in the n_1 direction break the translational symmetry and thereby relax the strict selection rules found in Section IV, A. As a consequence, the spectra in the current case have many more peaks than the few resulting from the three superradiant states in Section IV, A. For a simple linear aggregate, this effect of the boundary conditions is well-known.[33] Of course, for N_1 large, the current spectra simplify in structure and do not differ from the ones with periodic boundary conditions (if one there restricts to effective nearest-neighbor interactions as well), due to the fact that the optically dominant states get very close in energy, so that their line shapes merge. We finally note that the helical term in the CD spectrum, which in the case of periodic boundary conditions for N_1 large could be written as a derivative line shape ($dF/d\omega$), cannot be rewritten in such a simple form in the present case.

V. Numerical Results and Discussion

In this section, we present results for the linear absorption, LD, and CD spectra obtained by numerical diagonalization, taking into account all dipole−dipole interactions (eq 4) between the molecules on the cylinder. We will in particular be interested in the N_1 dependence of the spectra and the convergence toward the spectra obtained using periodic boundary conditions if N_1 becomes large.

As a model for our cylinders, we will use the structural model proposed for the rod elements of chlorosomal antennae of green bacteria consisting of BChl molecules.[13−16] For *C. aurantiacus*, the cylinders consist of BChl *c*. They have a radius $R = 2.297$ nm (with respect to the Mg atoms in the BChls) and a length that may extend to hundreds of nanometers. The other parameters taken from ref 14 translate into $N_2 = 6$, $h = 0.216$ nm, $\beta = 36.7°$, $\alpha = 189.6°$ (in ref 14, this angle was misplaced by its complement),[49] and $\gamma = 20°$. In the language of Holzwarth and co-workers, the cylinder consists of 18 parallel linear stacks of molecules, placed regularly around the cylinder with their axes parallel to the *z*-axis. The distance between molecules on a single stack is 0.648 nm, while neighboring stacks are shifted along the axis over $h = 0.216$ nm, implying that the molecules in different stacks line up exactly only once every third stack. This pattern is the one displayed in Figure 1, except that the angle between the stacks (i.e., the $\mathbf{a}_1$ direction) and the *z*-axis is 0° in the present case. Clearly, the cylinder symmetry does not hold for multiples of 20° rotation around the *z*-axis but only for multiples of 60°. In our language, the cylinder consists of six helices (which in Figure 1 run parallel to the $\mathbf{a}_2$ vector), winding at regular distances around the cylinder and having a pitch of 3.89 nm. Molecules reside at positions defined by the intersection of the helices with rings that are located at distances $h = 0.216$ nm on the cylinder. It should be kept in mind that a cylinder consisting of six helices and N_1 rings in our language consists of 18 stacks, each with $N_1/3$ molecules, in the language of Holzwarth and co-workers. We finally note that when calculating the various spectra, we have taken the transition frequency ω_0 of a single BChl *c* molecule to agree with a wavelength of 675 nm,[50−53] while we used for the dipole squared of a single molecule $\mu^2 \approx 20$ Debye^2. The latter value was obtained from the integrated extinction coefficient of monomeric solutions of BChl *c*[50,52,53], using the expression from ref 51.

Using the above model and parameters, we have numerically calculated $A(\omega)$ (eq 19), $LD(\omega)$ (eq 24), and $CD(\omega)$ (eq 31), keeping all dipole−dipole interactions within the cylinder. To facilitate the comparison with experiment, we will present the calculated spectra on a wavelength scale. We thus use $A(\lambda) = A(\omega)\, d\omega/d\lambda$ and analogous for the LD and the CD. The resulting spectra are shown in Figures 3−5 for various lengths N_1 of the cylinder. The solid lines are the spectra after using for the broadening function $F(\omega)$ a Gaussian with a full width at half-maximum (fwhm) of 500 cm^{-1}, chosen to reproduce the experimental absorption line width (vide infra). The units on the vertical axes have been taken the same ($N\mu^2$/nm) in all figures. Also shown are the stick spectra that give the positions of the original frequency δ functions and their strength. Dotted lines correspond to states falling in the $k_2 = 0$ band, while the dashed lines derive from the $k_2 = \pm 1$ bands (the strengths due to these degenerate bands have been added at each position). To fit on the same scale as the continuous spectra, the stick spectra are plotted in units of $30N\mu^2$ for the linear absorption and the LD spectra and $110N\mu^2$ for the CD spectra. We remind the reader that the total intensity of the linear absorption should be $N\mu^2/3$ as a consequence of the orientational averaging.

We first consider the absorption spectra (Figure 3). We see that all spectra are red-shifted relative to the monomer spectrum, which is due to the fact that the dominant transfer interaction is negative (J aggregate). This dominant interaction is the one between adjacent molecules within one stack, which we will denote $J_1 \equiv J(n_1 = 3, n_2 = -1) \approx -340$ cm^{-1}. Also, the next strongest interaction is negative, $J(n_1 = 2, n_2 = -1) \approx -190$ cm^{-1}, while the third one is positive, $J(n_1 = 1, n_2 = 0) \approx 109$ cm^{-1} (the interaction between nearest neighbors on one helix). We see that under each absorption peak states from both the $k_2 = 0$ and the $k_2 = \pm 1$ bands are hidden. This is due to the fact that the separation $\delta_\perp$ between these two bands is small as compared to the line broadening that we added. Using the solution for periodic boundary conditions, eq 33, we may estimate $\delta_\perp = E_h - E_0 \approx 168$ cm^{-1} (9 nm) in the limit of long cylinders. This is in good agreement with the typical energy separation between the dominant $k_2 = 0$ and the $k_2 = \pm 1$ transitions observed in Figure 3, even for the smaller cylinder lengths.

We also observe from Figure 3 that for N_1 small, the absorption band has a pronounced small-wavelength wing. This results from the fact that for small N_1 both in the $k_2 = 0$ and in the $k_2 = \pm 1$ bands the longitudinal wave functions $\varphi_{k_1}(n_1; k_2)$ that carry the oscillator strength have an energy separation of the same order of magnitude as the added line width of 500 cm^{-1}. This is clearly visible in the stick spectra of Figure 3a. The typical separation between peaks associated with different longitudinal quantum numbers may again be estimated from the solution for periodic boundary conditions. Keeping only the strongest interaction, we arrive at $\delta_{||} = E_{1,0} - E_{0,0} \approx 4\pi^2|9J_1|/N_1^2$. For $N_1 = 15$, this amounts to $\delta_{||} \approx 537$ cm^{-1} or 25 nm, which is in good agreement with the observed separation between the dominant states in the center of the band of Figure 3a and the weaker ones in the wing and indeed is comparable to the added line width. For increasing N_1, $\delta_{||}$ decreases and quickly becomes smaller than this width, as is clearly seen from the evolution of the stick spectra in Figure 3. As a result, the pronounced low-wavelength wing is seen to disappear.

For increasing N_1, the position and width of the absorption peak quickly converge to about 740 and 30 nm, respectively, which both are in good agreement with experimental spectra.[5,6,12] The fact that the line shape is rather insensitive to N_1 makes it hard to obtain solid information concerning the cylinder length from absorption measurements. Also, the position of the absorption maximum cannot easily be used as a measure for the length, because both the value of the single molecule transition frequency in the matrix of the chlorosomes and its transition dipole are subject to uncertainty.

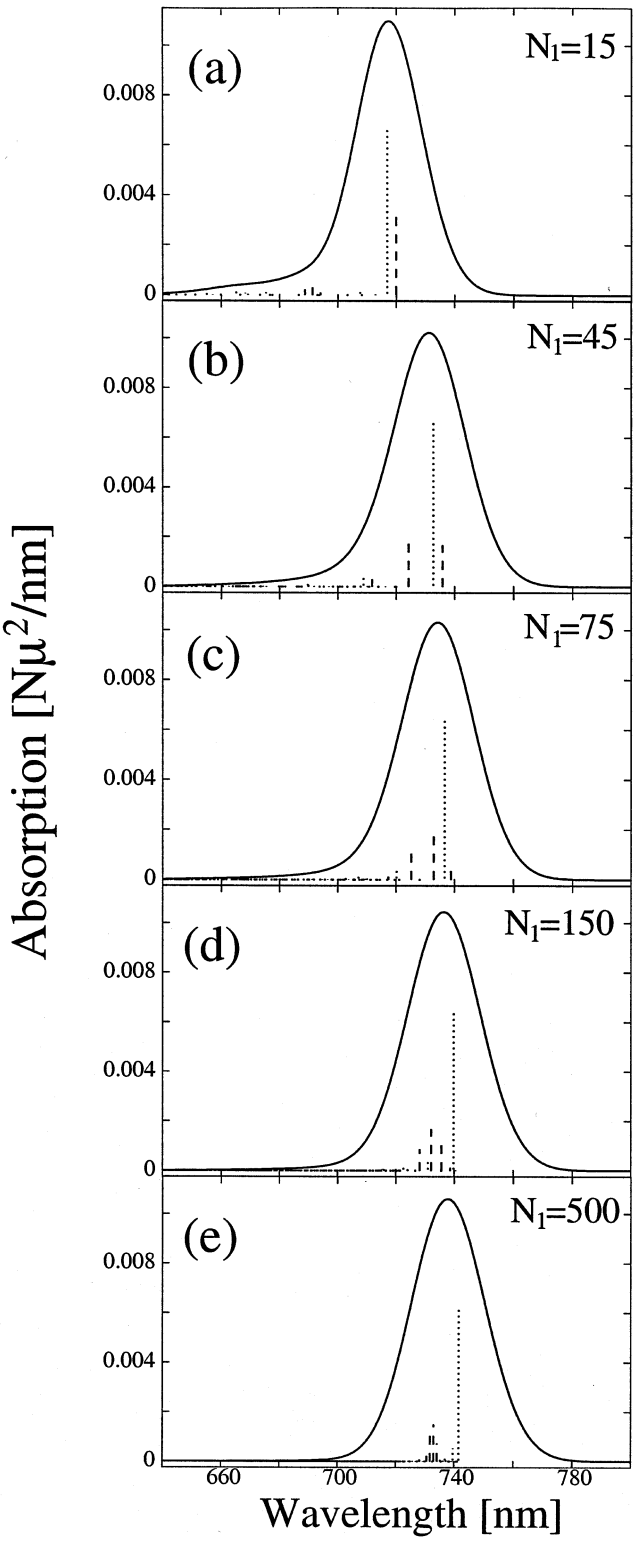

Figure 3. Linear absorption spectra calculated for cylindrical aggregates with a geometry applicable to the rod elements in the chlorosomes of *C. aurantiacus* (see text for details). The stick spectra were calculated using eq 19, with the dotted and dashed lines corresponding to the contributions from the $k_2 = 0$ and the $k_2 = \pm 1$ bands, respectively, while the solid lines are obtained by convoluting the stick spectra with a Gaussian with fwhm of 500 cm^{-1}. All spectra were converted to a wavelength scale. The stick spectra are given in units of $30N\mu^2$, while the continuous spectra have units $N\mu^2$/nm. The panels only differ in the choice of the cylinder length, for which we used the values $N_1 = 15$ (a), 45 (b), 75 (c), 150 (d), and 500 (e). We emphasize that a cylinder of N_1 rings corresponds to 18 stacks of $N_1/3$ molecules in the language of Holzwarth and co-workers.[13,14]

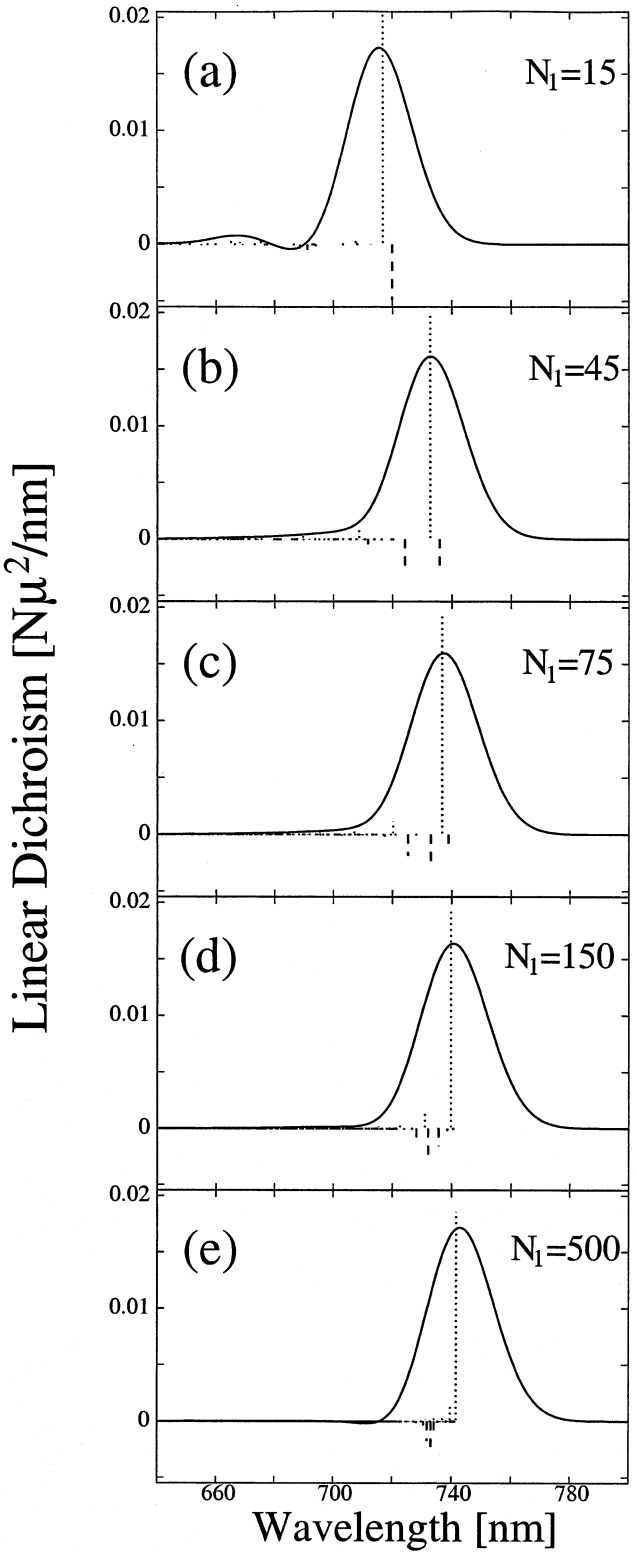

Figure 4. As in Figure 3, but now for the LD spectra, calculated using eq 24.

We next turn to the LD spectrum, which has positive and negative contributions associated with transitions in the $k_2 = 0$ and $k_2 = \pm 1$ bands, respectively (Figure 4). The main feature is positive; it is generally somewhat narrower than the main absorption peak of Figure 3, due to the canceling contribution of negative peaks at slightly smaller wavelengths. The resultant negative peak is seen to have a very small weight as compared to the positive peak. In fact, a (very small) net negative peak can only be discerned for $N_1 = 15$ and $N_1 = 500$. In

experimental LD spectra, a negative feature is never observed on the blue side of the main peak.[2−6] Instead, the experimental LD line shape closely follows the experimental absorption line shape, with a decreased weight at the low-wavelength side of the main LD peak as the only difference as compared to the absorption peak,[6] suggesting that indeed the important negative contributions lie there. Our theoretical LD and absorption line shapes in fact differ more from each other than in experiment. A possible explanation is that the angle β, which we used (taken from refs 13 and 14), overestimates the real value. Smaller angles (10−30°) have in fact been suggested by various authors.[4−6] We will come back to this point below.

We next turn to the CD spectra (Figure 5), which have been the subject of most discussion in the literature (see Introduction). As is seen, the CD spectrum changes strongly in shape for cylinder lengths of up to $N_1 \approx 100$; the changes are much more dramatic than the variation of the absorption and the LD with N_1. This fact has first been noted by Prokhorenko and Holzwarth.[22] Using the separation of the various CD contributions, which we introduced below eq 31, this strong variation may easily be understood. We see that three types of contributions determine the CD spectrum. The $k_2 = 0$ band contributes only ring type contributions, which are negative for the chlorosome geometry ($\alpha = 189.6°$ and $\beta = 36.7°$). The dominant states in this band are found in a region with characteristic width $\delta_{||} \approx 4\pi^2|9J_1|/N_1^2$. The $k_2 = \pm 1$ bands give positive ring contributions, again mainly in an energy region of width $\delta_{||}$, which, however, has its center separated from the $k_2 = 0$ region of the spectrum by an amount $\delta_\perp = E_h - E_0 \approx 168\ \mathrm{cm}^{-1}$. At the same time, the $k_2 = \pm 1$ bands give dispersive helical contributions. These three types of contributions have been indicated in Figure 6. From this, we clearly see that the relative positions of positive and negative contributions may strongly vary with varying N_1. In particular, for small N_1, $\delta_{||}$ exceeds $\delta_\perp$, so that the dominant regions of the $k_2 = 0$ and $k_2 = \pm 1$ bands strongly overlap, causing a large variability of the relative position of positive and negative peaks with only small changes in N_1. On the other hand, for N_1 large, the dominant regions of the $k_2 = 0$ and $k_2 = \pm 1$ bands have separated, and the negative ring contributions concentrate completely on the high-wavelength side of the spectrum, while the positive and dispersive contributions collect at the small-wavelength side. This is clearly seen in Figure 5e, where the spectrum has become almost independent of N_1. In conclusion, we found that the strong variation of the calculated spectrum with changing N_1 is a consequence of the extreme sensitivity of the overlap between the $k_2 = 0$ and the $k_2 = \pm 1$ bands to the length of the cylinder. This conclusion may in fact be generalized to include a sensitivity to the variation of other geometrical parameters that affect the details of the bandwidth, such as the various angles (α, β) and the circumference N_2 of the cylinder. As to the variability of measured CD spectra,[2−10] we believe, however, that the variation of the length (or the exciton localization length along the cylinder axis) is the most likely explanation, as the other parameters are intimately related to the self-assembly of the BChl molecules in the cylinder.

We note that the variation of the experimentally observed CD spectra is nicely recovered in the various spectra of Figure 5. For example, the spectra presented in Figure 2 of ref 5 or the spectra 5 and 6 in Figure 4 of ref 6 resemble our Figure 5c, while spectra as in Figure 2 of ref 7, Figure 7 of ref 8, or the spectra 3 and 4 in Figure 4 of ref 6 resemble our spectra Figure 5d,e. These two types of spectra (one with a single peak and a blue-shifted dip and the other with a single peak separating two

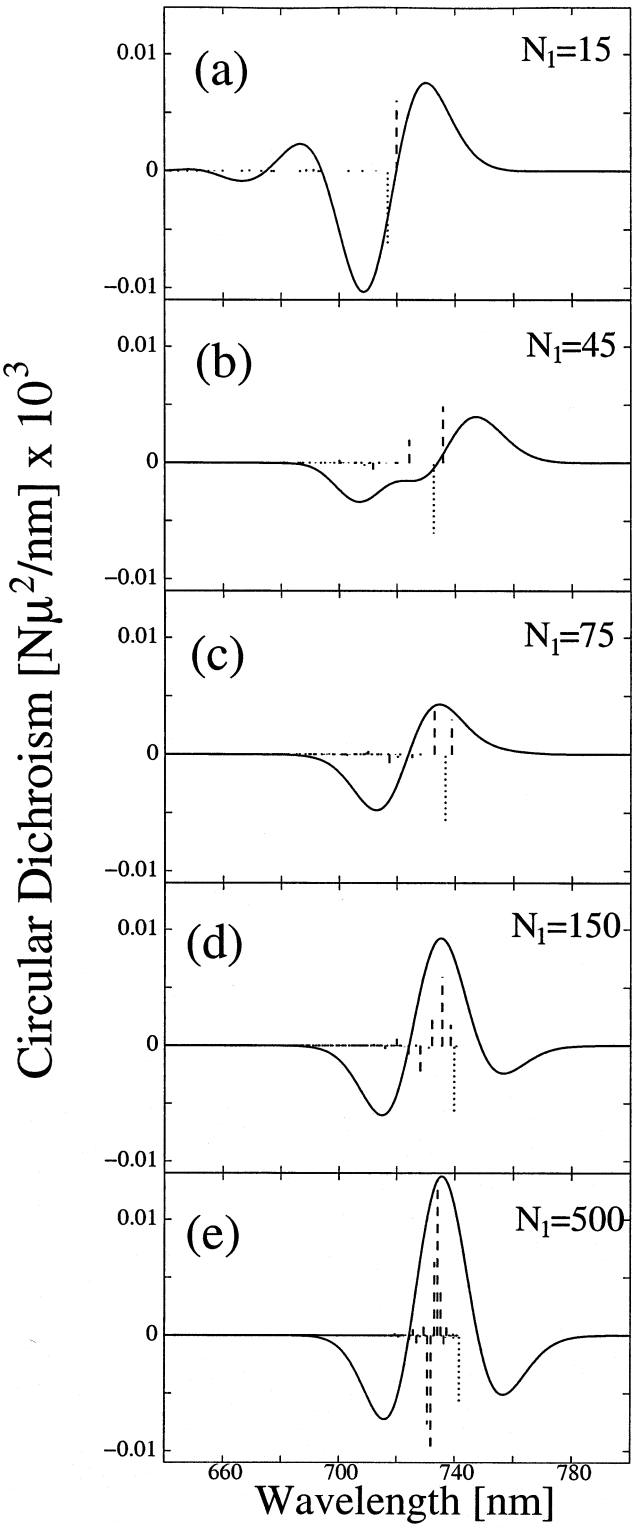

Figure 5. As in Figure 3, but now for the CD spectra, calculated using eq 31. The stick spectra are now given in units of $110N\mu^2$.

dips) seem to cover most experiments. In fact, some experimental evidence exists for the fact that a size variation may be responsible for the typical changes of the CD spectrum upon using different sample preparation routes. In ref 10, it was reported that chlorosomes with a length of 110 ± 18 nm have a CD spectrum that closely resembles our spectra for relatively short cylinder sizes (Figure 5c), while chlorosomes with lengths of 220 ± 70 have a CD that is very similar to our spectra for larger N_1 (Figure 5d,e). In ref 10 (and also ref 6), this second

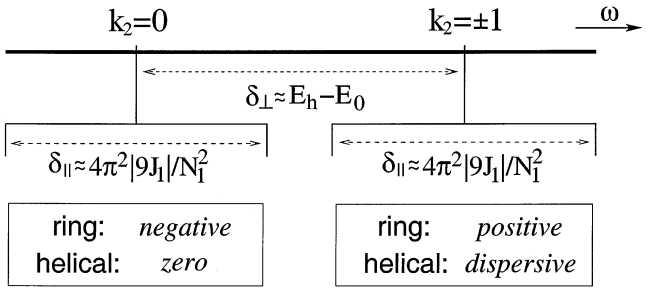

Figure 6. Schematic indication of the various CD contributions, their origin, and the frequency range in which they predominantly occur. For N_1 small, the $k_2 = 0$ and $k_2 \pm 1$ contributions may overlap and (partially) cancel each other, giving rise to a strong dependence of the CD spectrum to the precise value of N_1.

type of CD has a high-wavelength dip that is stronger than the low-wavelength dip, a situation that is not encountered in our calculations. Preliminary calculations show that the inclusion of continuous energy disorder as a source of line broadening lifts this discrepancy between theory and experiment. We thus see that a variation of the length of the chlorosomes may explain the typical variation in shape of the CD spectrum observed in experiment. We also stress that this change of the CD spectrum between Figure 5c and 5d,e is not accompanied by an observable change in the absorption line shape and position (Figure 3c−e). This, too, is in agreement with the experimental situation: various sample preparation routes lead to negligible changes in the absorption spectra. As far as we know, CD spectra resembling Figure 5a,b have not been observed experimentally, probably because chlorosomes do not occur in such small sizes.

While the above nicely explains the general variability of measured CD spectra, the theoretical and experimental results in fact do differ in some respects. First, as noted above already, the difference between the theoretical absorption and the LD line shapes is generally somewhat larger than observed in experiment. Second, experimental CD spectra of the type Figure 5c typically show their positive peak to be red-shifted relative to the positive peak in the spectra of the type Figure 5d,e. This is not the case in the theoretical spectra. Third, the size at which the transition between both types of CD spectra occur in Figure 5 is rather small ($N_1 \approx 100$ rings, which agrees with a length of about 20 nm). It turns out that these problems may be solved if we allow for a smaller value of the angle β. In fact, several authors have suggested that this angle may be smaller than the value of 36.7° obtained in the molecular dynamics simulations of refs 13 and 14. Values in the range of 10−30° have been reported.[4−6] In Figure 7, we present absorption, LD, and CD spectra for cylinders with the same parameters as used in Figures 3−5, except that we used $\beta = 25°$ and the value of ω_0 was changed to 666 nm in order to keep the absorption line at 740 nm. The change between the two main types of CD spectra now occurs at cylinders of a few hundred rings, while we also see that the other two noted discrepancies with the experiment have disappeared. The N_1 value at which the transition between the two main types of CD occurs is to a large extent determined by the energy scale $\delta_\perp$: the transition to the form with one peak and two dips is complete after the (optically dominant states in) the bands with $k_2 = 0$ and $k_2 = \pm 1$ have completely separated (cf. Figure 6). The smaller $\delta_\perp$ is, the larger the transition value for N_1 will be. For $\beta = 25°$, we have $\delta_\perp = 84$ cm^{-1} = 4.5 nm, which is about twice as small as $\delta_\perp$ for $\beta = 36.7°$. This explains the larger cylinder length at which the transition occurs.

To end this section, we study the convergence of the numerically calculated spectra to the analytical results obtained

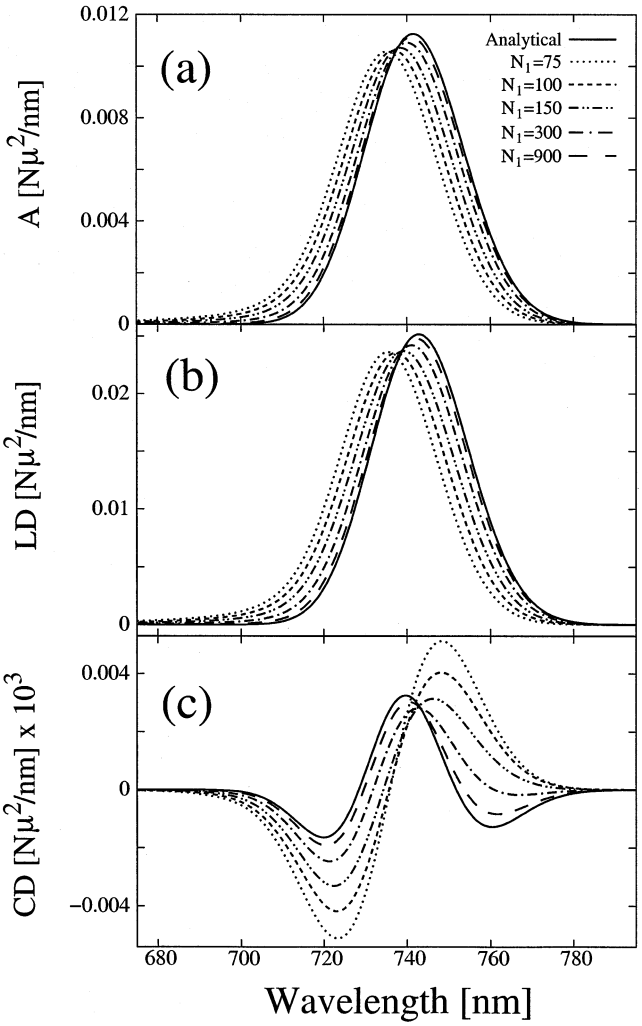

Figure 7. (a) Convergence of the absorption spectrum for growing cylinder length N_1 to the analytical result obtained for periodic boundary conditions (solid line). (b) Idem for the LD spectrum. (c) Idem for the CD spectrum. Cylinder geometry and units of the spectra are as in Figure 3, except that $\beta = 25°$ and ω_0 was chosen to agree with a wavelength of 666 nm.

using periodic boundary conditions. This convergence is nicely illustrated in Figure 7 as well (for $\beta = 36.7°$, very similar convergence plots are found). Clearly, all spectra properly converge to the analytical results. For the absorption and LD spectra, the shape has completely converged for $N_1 \approx 50$ (not shown). Their position still undergoes a small shift for larger N_1, which is due to the long-range nature of the dipole−dipole interactions. Shape convergence should occur for values of N_1 for which $\delta_{||}$ is much smaller than the line width of the broadening function $F(\omega)$, which translates for our line width of 500 cm^{-1} into $N_1 \gg 16$. We observe from Figure 7c that the convergence for the CD spectra is considerably slower than for the absorption and the LD. This is due to the fact that the CD line shape sensitively depends on the relative positions of positive and negative contributions. Even small changes in these positions, which may still occur at large N_1, cause substantial changes in the spectra. This sensitivity has the same origin as the already discussed extreme sensitivity of the qualitative features of the CD spectrum to the cylinder length at smaller N_1 values. We note in passing that for the current geometry, the group velocity $v_h(\gamma)$ is negative, so that the last (helical) term in eq 45 has its positive peak at the high wavelength side and its dip at the low wavelength side. Together with the $k_2 =$

± 1 positive ring contributions at $\omega = E_h$, this gives the S-shaped part of the solid spectrum centered at about 730 nm in Figure 7c. The $k_2 = 0$ negative ring contribution at $\omega = E_0$ is responsible for the dip at about 755 nm in the solid spectrum in Figure 7c.

As the strongest dipole−dipole interaction, $J_1 = J(n_1 = 3, n_2 = -1)$ in the system occurs between molecules that are three rings apart; it is of little use to compare the numerical results for the chlorosome geometry to the analytical ones derived for effective nearest-neighbor ring interactions (Section IV, B).

VI. Concluding Remarks

In this paper, we have theoretically studied the absorption, LD, and CD spectra for cylindrical molecular aggregates with a helical structure. We have first shown how such aggregates may in general be constructed from an arbitrary 2D lattice and how we may view them as a perpendicular stack of N_1 rings, intersected by N_2 helices, the intersection points giving the positions of the molecules (Figure 2). This view has helped us to decompose the system into a set of N_2-decoupled effective 1D Frenkel exciton systems, each characterized by a transverse wavenumber k_2. Only states with $k_2 = 0$ and $k_2 = \pm 1$ contribute to the linear spectra studied here; the bands with $k_2 = \pm 1$ contribute equal amounts (degeneracy). This decomposition has also allowed us to distinguish quite generally between three types of CD contributions: (i) ring contributions resulting from the $k_2 = 0$ band, (ii) ring contributions resulting from the $k_2 = \pm 1$ bands, and (iii) helical contributions caused by states in the $k_2 = \pm 1$ band. The first two have opposite signs, while the helical contribution has a dispersive shape. From our analytical solution for periodic boundary conditions (long cylinders), we have found that the group velocity of the excitons plays an important role in the dispersive term. The same analytical solution indicates that for long cylinders all oscillator strength is contained in three superradiant states, one that is polarized along the cylinder axis and has constant amplitude on all molecules (zero wavevector) and two that are polarized perpendicular to the axis, with wavevectors that are dictated by the circumference and the helicity of the cylinder. Using numerical diagonalizations, we have shown that for long cylinders the exact spectra properly converge toward the analytical ones. The convergence is slowest for the CD spectrum, owing to a delicate interference between the various positive and negative contributions.

We have compared our model calculations to the experimental spectra for the rod elements of the chlorosomal antenna systems of green bacteria, using the aggregate geometry proposed in refs 13 and 14. We have found in particular that the observed strong variation of the measured CD spectra with sample preparation[2,3,5−10] (while keeping the absorption and LD spectra unchanged) may be explained from a strong sensitivity of the CD spectrum to the overlap of the various positive and negative CD contributions in the $k_2 = 0$ and the $k_2 = \pm 1$ bands (Figure 6). This overlap is very sensitive to the length and circumference of the cylinder. In addition, the overlap is affected by relatively small changes in the angles α and β, which explains the sensitivity of the CD spectra to α found in ref 30. In the self-assembled chlorosomes with a tight network of hydrogen bonds, a variation of length (or exciton delocalization length) with sample preparation seems more likely than a variation of the structural angles. In addition, an explanation of the CD variability based on variation of the angles α and β in various preparation techniques would also predict the absorption and LD peak position to change, a fact that contradicts experimental observation. Our explanation based on N_1 variation keeps these positions fixed. The fits of our spectra to the experiment suggest that the angle β may be smaller than the 36.7° predicted by molecular dynamics calculations.[13,14] We find better agreement with the experiment for $\beta = 25°$. A more detailed study of the role of continuous energy disorder may shed further light on this matter.

We finally notice that two aspects of our model study deserve future attention. First, we have included line broadening in a simple way, by convoluting stick spectra with Gaussian line shapes. While we believe that this allows us to describe the salient features of the spectra, it is of interest to consider in more detail the situation with continuous disorder in the transition energies and (or) transfer interactions and the concomitant localization of the states on the cylinders. In particular, it will be of interest to investigate the separation of the states into bands characterized by $|k_2|$ and the possibility for states to delocalize around the cylinder, while localizing in the longitudinal direction. The second limitation is that we have assumed the linear dimensions of the cylinders to be short as compared to the relevant optical wavelength. While for chlorosomes this typically seems to hold, previous (classical) studies have indicated that in particular the CD spectrum may strongly change for sizes larger than the wavelength (psi type anomalies).[54]

Acknowledgment. We thank Prof. Dr. A. R. Holzwarth and Dr. V. I. Prokhorenko for many stimulating discussions. This work is part of the research program of the Stichting voor Fundamenteel Onderzoek der Materie (FOM), which is financially supported by the Nederlandse Organisatie voor Wetenschappelijk Onderzoek (NWO).

References and Notes

(1) Staehelin, L. A.; Golecki, J. R.; Drews, G. *Biochim. Biophys. Acta* **1980**, *589*, 30.
(2) Betti, J. A.; Blankenship, R. E.; Natarajan, L. V.; Dickenson, L. C.; Fuller, R. C. *Biochim. Biophys. Acta* **1982**, *680*, 194.
(3) van Dorssen, R. J.; Vasmel, H.; Amesz, J. *Photosynth. Res.* **1986**, *9*, 33.
(4) van Amerongen, H.; Vasmel, H.; van Grondelle, R. *Biophys. J.* **1988**, *54*, 65.
(5) Frese, R.; Oberheide, U.; van Stokkum, I.; van Grondelle, R.; Foidl, M.; Oelze, J.; van Amerongen, H. *Photosynth. Res.* **1997**, *54*, 115.
(6) Griebenow, K.; Holzwarth, A. R.; van Mourik, F.; van Grondelle, R. *Biochim. Biophys. Acta* **1991**, *1058*, 194.
(7) Steensgaard, D. B.; van Walree, C. A.; Permentier, H.; Bañeras, L.; Borrego, C. M.; Garcia-Gil, J.; Aartsma, T. J.; Amesz, J.; Holzwarth, A. R. *Biochim. Biophys. Acta* **2000**, *1457*, 71.
(8) Wang, Z. Y.; Marx, G.; Umetsu, M.; Kobayashi, M.; Mimuro, M.; Nozawa, T. *Biochim. Biophys. Acta* **1995**, *1232*, 187.
(9) Olson, J. M.; Gerola, P. D.; van Brakel, G. H. In *Antennas and Reaction Centers of Photosynthetic Bacteria*; Michel-Beyerle, M. E., Ed.; Series in Chemical Physics, Vol. 42; Springer: New York, 1985; p 67.
(10) Lehmann, R. P.; Brunisholz, R. A.; Zuber, H. *Photosynth. Res.* **1994**, *41*, 165.
(11) Fetisova, Z. G.; Mauring, K. *FEBS Lett.* **1992**, *307*, 371.
(12) Savikhin, S.; Buck, D. R.; Struve, W. S.; Blankenship, R. E.; Taisova, A. S.; Novoderezhkin, V. I.; Fetisova, Z. G. *FEBS Lett.* **1998**, *430*, 323.
(13) Holzwarth, A. R.; Schaffner, K. *Photosynth. Res.* **1994**, *41*, 225.
(14) Prokhorenko, V. I.; Steensgaard, D. B.; Holzwarth, A. R. *Biophys. J.* **2000**, *79*, 2105.
(15) Balaban, T. S.; Holzwarth, A. R.; Schaffner, K. *J. Mol. Struct.* **1995**, *349*, 183.
(16) van Rossum, B. J.; Boender, G. J.; Mulder, F. M.; Raap, J.; Balaban, T. S.; Holzwarth, A. R.; Schaffner, K.; Prytulla, S.; Oschkinat, H.; de Groot, H. J. M. *Spectrochim. Acta A* **1998**, *54*, 1167.
(17) Pawlik, A.; Kirstein, S.; De Rossi, U.; Daehne, S. *J. Phys. Chem. B* **1997**, *101*, 5646.
(18) Kirstein, S.; von Berlepsch, H.; Böttcher, C.; Burger, C.; Ouart, A.; Reck, G.; Daehne, S. *CHEMPHYSCHEM* **2000**, *3*, 146.
(19) Spitz, C.; Knoester, J.; Ouart, A.; Daehne, S. *Chem. Phys.* **2002**, *275*, 271.

(20) Bednarz, M.; Knoester, J. *J. Phys. Chem. B* **2001**, *105*, 12913.
(21) Lampoura, S. S.; Spitz, C.; Daehne, S.; Knoester, J.; Duppen, K. *J. Phys. Chem. B* **2002**, *106*, 3103.
(22) Prokhorenko, V. I.; Holzwarth, A. R. Private Communication and *Biophys. J.* Submitted for publication.
(23) von Berlepsch, H.; Kirstein, S.; Böttcher, C. *Langmuir* **2002**, *18*, 7699.
(24) Daehne, S.; Nolte, K.-D. *Chem. Commun.* **1972**, 1056.
(25) Mees, C. E. K. *The Theory of the Photographic Process*; The MacMillan Company: New York, 1962.
(26) Herz, A. H. *Adv. Colloid Interface Sci.* **1977**, *8*, 237.
(27) Tani, T. *Photographic Sensitivity*; Oxford University Press: Oxford, 1995.
(28) Didraga, C.; Knoester, J. *Chem. Phys.* **2002**, *275*, 307.
(29) Koolhaas, M. H. C.; Frese R. N.; Fowler, G. J. S.; Bibby, T. S.; Georgakopoulou, S.; van der Zwan, G.; Hunter, C. N.; van Grondelle, R. *Biochemistry* **1998**, *37*, 4693.
(30) Somsen, O. J. G.; van Grondelle, R.; van Amerongen, H. *Biophys. J.* **1996**, *71*, 1934.
(31) Fetisova, Z.; Freiberg, A.; Mauring, K.; Novoderezhkin, V.; Taisova, A.; Timpmann, K. *Biophys. J.* **1996**, *71*, 995.
(32) Knapp, E. W. *Chem. Phys.* **1984**, *85*, 73.
(33) Fidder, H.; Knoester, J.; Wiersma, D. A. *J. Chem. Phys.* **1991**, *95*, 7880.
(34) Knoester, J. *J. Chem. Phys.* **1993**, *99*, 8466.
(35) Avetisyan, Y. A.; Zaitsev, A. I.; Malyshev V. A. *Opt. Spektr*. **1985**, *59*, 967 (*Opt. Spectrosc.* **1985**, *59*, 582).
(36) Spano, F. C.; Mukamel, S. *J. Chem. Phys.* **1989**, *91*, 683.
(37) de Boer, S.; Wiersma, D. A. *Chem. Phys. Lett.* **1990**, *165*, 45.
(38) Chesnut, D. B.; Suna, A. *J. Chem. Phys.* **1963**, *39*, 146.
(39) Juzeliūnas, G. *Z. Phys. D* **1988**, *8*, 379.
(40) Spano, F. C. *Phys. Rev. Lett.* **1991**, *67*, 3424.
(41) Malyshev, V. A. *Opt. Spektr*. **1991**, *71*, 873 (*Opt. Spectrosc.* **1991**, *71*, 505); *J. Lumin.* **1993**, *55*, 225.
(42) Bakalis, L. D.; Knoester, J. *J. Phys. Chem. B* **1999**, *103*, 6620.
(43) Malyshev, A. V.; Malyshev, V. A. *Phys. Rev. B* **2001**, *63*, 195111.
(44) Saito, R.; Dresselhaus, G.; Dresselhaus, M. S. *Physical Properties of Carbon Nanotubes*; Imperial College Press: London, 1998.
(45) Davydov, A. S. *Theory of Molecular Excitons*; Plenum: New York, 1971.
(46) Agranovich, V. M.; Galanin, M. D. In *Electronic Excitation Energy Transfer in Condensed Matter*; Agranovich, V. M., Maradudin, A. A., Eds.; North-Holland: Amsterdam, 1982.
(47) Born, M.; Wolf, E. *Principles of Optics*; Pergamon Press: Oxford, 1980.
(48) Jackson, J. D. *Classical Electrodynamics*; John Wiley: New York, 1975.
(49) Prokhorenko, V. I. Private communication.
(50) Frigaard, N. U.; Larsen, K. L.; Cox, R. P. *FEMS Microbiol. Ecol.* **1996**, *20*, 69.
(51) Houssier, C.; Sauer, K. *J. Am. Chem. Soc.* **1970**, *92*, 779.
(52) Umetsu, M.; Wang, Z. Y.; Kobayashi, M.; Nozawa, T. *Biochim. Biophys. Acta* **1999**, *1410*, 19.
(53) Dudkowiak, A.; Francke, C.; Amesz, J.; Planner, A.; Hanyż, I.; Frąckowiak, D. *Spectrochim. Acta A* **1996**, *52*, 251.
(54) Keller, D.; Bustamante, C. *J. Chem. Phys.* **1984**, *84*, 2972.